J. Plasma Phys. (2026), *vol*. 92, E101 © The Author(s), 2026. Published by Cambridge University Press.
This is an Open Access article, distributed under the terms of the Creative Commons Attribution licence (https://creativecommons.org/licenses/by/4.0/), which permits unrestricted re-use, distribution and reproduction, provided the original article is properly cited.doi:10.1017/S0022377826101998

Firewall effect on electron acceleration by R-waves and parallel electric fields

Hye Lin Kang[1], Young Dae Yoon[1,2,†], Myung-Hoon Cho[3] and Gunsu S. Yun[1,4]

[1]Department of Physics, Pohang University of Science and Technology, Pohang, Republic of Korea
[2]Asia Pacific Center for Theoretical Physics, Pohang, Republic of Korea
[3]Pohang Accelerator Laboratory, Pohang University of Science and Technology, Pohang, Republic of Korea
[4]Division of Advanced Nuclear Engineering, Pohang University of Science and Technology, Pohang, Republic of Korea

Corresponding authors: Young Dae Yoon, ydyoon@physics.ucla.edu; Gunsu S. Yun, gunsu@postech.ac.kr

(Received 8 April 2026 UTC; revision received 11 May 2026 UTC; accepted 5 June 2026 UTC)

We report an unanticipated electron dynamics in a classical setting of a uniform magnetic field, a parallel electric field and a right-handed circularly polarised wave (R-wave). The setting admits a natural trajectory that a particle accelerated by the electric field reaches a Doppler–shifted cyclotron resonance and becomes trapped in the resonance space. Remarkably, once it becomes resonantly trapped, the electron undergoes reversal of parallel acceleration together with perpendicular energisation, despite the parallel electric field remaining constant. This counterintuitive behaviour has important implications for particle scattering in various laboratory and space plasmas. Applied to fusion devices, particle-in-cell simulations show that an externally injected R-wave can act as a firewall suppressing further runaway-electron acceleration.

Key words: plasma dynamics, fusion plasma, space plasma physics

1. Introduction

Resonant interactions between charged particles and electromagnetic waves govern energetic-particle dynamics in various magnetised plasma environments. In fusion plasmas, controlling runaway electrons is a central challenge (Breizman *et al.* 2019; Salewski *et al.* 2025), and wave-induced momentum redirection offers a promising mitigation route (Zhou *et al.* 2011; Guo, McDevitt & Tang 2018;

[†]*Present address:* Department of Physics and Astronomy, University of California, Los Angeles, CA 90095, USA.

https://doi.org/10.1017/S0022377826101998 Published online by Cambridge University Press

Yoon, Ji & Yun 2021; Decker *et al.* 2024; Choudhury *et al.* 2026). Similar resonant mechanisms shape energetic-electron behaviour in space, producing solar-wind and flare-accelerated populations (Reames, Meyer & von Rosenvinge 1994; Vocks *et al.* 2005; Lacombe *et al.* 2014; Stansby *et al.* 2016), auroral emissions (Horne *et al.* 2003; Miyoshi *et al.* 2010; Kasahara *et al.* 2018) and radiation-belt losses (Inan *et al.* 2003; Sauvaud *et al.* 2008; Compernolle *et al.* 2014; Yoon & Bellan 2020). Energetic ions in tokamaks (Heidbrink & White 2020; Kirov *et al.* 2024) and stellarators (Siena, Navarro & Jenko 2020; Paul *et al.* 2022, 2023) likewise interact with Alfvénic and ion-cyclotron waves, leading to redistribution and confinement degradation. During magnetic reconnection, waves and energetic particles are simultaneously generated and thus mutually interact (Yoo *et al.* 2024; Park, Yoon & Hwang 2025). Many of these interactions occur through Doppler-shifted cyclotron resonance, which drives particle scattering in both quasilinear (Lyons 1974; Summers 2005; Pokol, Fülöp & Lisak 2008; Guo *et al.* 2018; Liu *et al.* 2018) and single-particle regimes (Bellan 2013; Yoon & Bellan 2020; Yoon *et al.* 2021).

These interactions in many cases involve an electric field parallel to the background magnetic field. For instance, parallel electric fields are responsible for runaway-electron generation in tokamaks (Connor & Hastie 1975; Helander, Eriksson & Andersson 2002; Marshall & Bellan 2019; Lee *et al.* 2024) and are also important during guide-field magnetic reconnection (Schindler, Hesse & Birn 1988; Richard *et al.* 2025). They are also readily observed in Earth's magneto/ionospheres (Gurnett 1972; Yeh & Hill 1981; Fälthammar 1989; Ergun *et al.* 2002) and in magnetic mirror devices (Geller *et al.* 1974; Burdakov, Ivanov & Kruglyakov 2010), where plentiful amounts of wave–particle interactions occur.

Previous studies have shown that the coexistence of parallel forces and resonant wave interactions can produce unconventional particle dynamics, mainly in the context of space plasmas. For example, Kuramitsu & Krasnoselskikh (2005*a*,*b*,*c*) demonstrated that when an electrostatic field profile maintains cyclotron resonance between a charged particle and a circularly polarised wave, substantial perpendicular energisation can occur, a process referred to as 'gyroresonant surfing'. Similarly, Omura *et al.* (2007) showed that the combined action of the magnetic mirror force and the whistler mode waves, one class of the R-waves, can lead to efficient electron acceleration through the mechanism known as 'relativistic turning acceleration'.

Despite these important advances, several limitations remain as regards previous studies. Kuramitsu & Krasnoselskikh (2005*a*,*b*,*c*) solved the non-relativistic equations of motion and modelled the evolution of the perpendicular velocity, assuming that the parallel velocity is continuously maintained at the Doppler resonance condition by a prescribed electrostatic field profile. Omura *et al.* (2007) considered only mirror-trapped electrons with sufficiently large perpendicular velocity and whose parallel velocity reaches zero. A generalised theory describing coherent wave–particle interaction under parallel forces is thus warranted.

In this paper, we perform a rigorous, exact theoretical treatment of the fully relativistic interaction between an electron and a right-handed circularly polarised wave (R-wave) in a constant parallel electric field by means of a pseudo-potential analysis (Bellan 2013). Far from Doppler-shifted cyclotron resonance, the parallel electric field accelerates the electron towards resonance. For a sufficiently strong wave amplitude the particle may be trapped near resonance, at which point it undergoes acceleration in the direction opposite to its prior motion as well as in the perpendicular direction. This reflection, which is absent in the non-relativistic limit, is schematically shown in figure 1. Although we focus on interactions between

https://doi.org/10.1017/S0022377826101998 Published online by Cambridge University Press

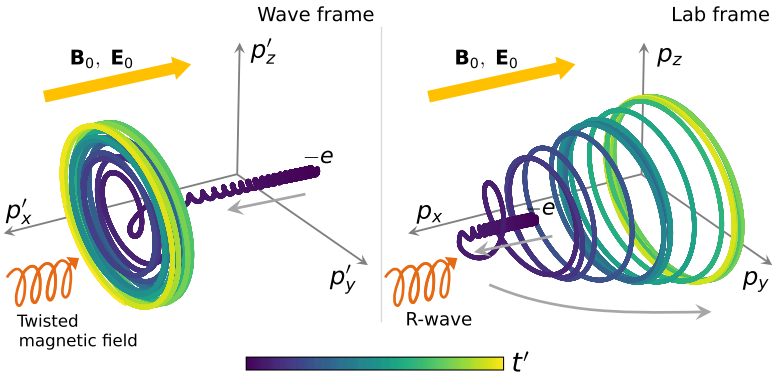


FIGURE 1. Schematic diagram of an electron trajectory in (left) the wave-frame and (right) the laboratory-frame momentum space under a uniform magnetic field, a parallel electric field and a right-handed circularly polarised wave (R-wave).

electrons and R-waves, the mechanism is fully generalisable to positively charged particles such as ions and L-waves. This counterintuitive analytical prediction is verified by single-particle simulations and further confirmed by self-consistent particle-in-cell (PIC) simulations using typical tokamak plasma parameters. We demonstrate that an externally applied wave can act as an acceleration firewall, preventing runaway electrons from accelerating beyond a prescribed momentum, as well as accelerating them in the perpendicular direction. Implications for other systems, including space, astrophysical and stellarator plasmas, are also discussed.

2. Electron motion in a coherent R-wave ($E_0 = 0$)

To sequentially introduce our analytical derivation, we first consider a negatively charged particle with rest mass m, charge $q < 0$ and momentum $\boldsymbol{p} = \gamma m \boldsymbol{v}$ subject to a coherent R-wave and a steady-state background magnetic field directed along the x axis:

$$\boldsymbol{B} = B_0 \left\{ \hat{x} + b[\hat{y} \sin(kx - \omega t) + \hat{z} \cos(kx - \omega t)] \right\},$$
$$\boldsymbol{E} = -\frac{\omega}{k} \hat{x} \times \boldsymbol{B}, \tag{2.1}$$

where b is the relative amplitude of the wave magnetic field, which is not necessarily small. The wave angular frequency ω, wavenumber k and b are assumed to be constant. Note that although we consider here a negatively charged particle under an R-wave, the dynamics is identical for a positively charged particle under an L-wave (Yoon & Bellan 2020).

In the frame moving with the wave phase velocity $v_{\mathrm{ph}} = \omega/k$, the electromagnetic fields and the equation of motion transform to

$$\boldsymbol{B}' = B_0\{\hat{x} + b'[\hat{y} \sin(k'x') + \hat{z} \cos(k'x')]\},$$
$$\boldsymbol{E}' = \boldsymbol{0}, \tag{2.2}$$

$$\frac{\mathrm{d}}{\mathrm{d}t'} \left(\frac{\boldsymbol{p}'}{mc} \right) = -\omega_{\mathrm{c}} \frac{\boldsymbol{p}'}{\gamma' mc} \times \frac{\boldsymbol{B}'}{B_0}, \tag{2.3}$$

https://doi.org/10.1017/S0022377826101998 Published online by Cambridge University Press

where $\omega_c = |qB_0/m|$ is the laboratory-frame cyclotron frequency and all the primed symbols indicate wave-frame variables. Specifically, $b' = b\sqrt{1-n^{-2}}$ and $k' = k\sqrt{1-n^{-2}}$, with the wave refractive index $n = ck/\omega = c/v_{ph}$. Therefore, in the wave frame, the electromagnetic fields reduce to a time-independent twisted magnetic field. Since $\boldsymbol{E}' = \boldsymbol{0}$, the particle energy in the wave frame is conserved; equivalently, the wave-frame particle Lorentz factor γ' is constant.

A dimensionless 'frequency mismatch parameter' is now introduced as

$$\begin{aligned}\xi &\equiv -\frac{\gamma}{\omega_c}\left(\omega - kv_x - \frac{\omega_c}{\gamma}\right),\\ &= 1 + \frac{ck'}{\omega_c}\frac{p'_x}{mc},\end{aligned} \tag{2.4}$$

which is zero at normal Doppler resonance $\omega - kv_x = \omega_c/\gamma$ and thus is a measure of how far the particle is away from this resonance. Because wave parameters are assumed to be constant, ξ is a characteristic of the particle, embodying information about its velocity, energy, pitch angle, etc., and so a change in ξ corresponds to changes in these particle parameters. Also, given the wave parameters, the resonant energy γ_r and resonant parallel momentum p_r can be calculated given the pitch angle α by solving $\xi = 0$.

The vector equations (2.2) and (2.3) can be exactly recast into a scalar equation for ξ (Bellan 2013), which describes an equation of motion of the particle's ξ in a pseudo-potential $\psi(\xi)$:

$$\frac{\gamma'^2}{\omega_c^2}\frac{\mathrm{d}^2\xi}{\mathrm{d}t'^2} = -\frac{\partial\psi(\xi)}{\partial\xi}, \tag{2.5}$$

where

$$\psi(\xi) = \frac{1}{8}\xi^4 + \frac{1}{2}\left(b'^2 - b'\frac{ck'}{\omega_c}\frac{p'_{z0}}{mc} - \frac{1}{2}\xi_0^2\right)\xi^2 - b'^2\xi, \tag{2.6}$$

and subscript 0 indicates initial conditions at $t = t' = 0$, and the initial particle position $x(t=0) = 0$ was assumed without loss of generality. Equation (2.6) shows that the pseudo-potential is a quartic function of ξ, and its coefficients are determined by wave parameters and particle initial conditions.

From (2.5), one can derive the conservation of pseudo-energy:

$$\frac{1}{2}\left(\frac{\gamma'}{\omega_c}\frac{\mathrm{d}\xi}{\mathrm{d}t'}\right)^2 + \psi(\xi) = \text{const.}, \tag{2.7}$$

which illustrates the conservative motion of the particle in $(\xi, \mathrm{d}\xi/\mathrm{d}t')$ space.

3. Parallel electric field effects ($E_0 \neq 0$)

Now, we add a finite steady-state electric field $\boldsymbol{E} = \boldsymbol{E}' = E_0\hat{x}$. To reduce notational clutter, we define normalised quantities $\bar{t} = \omega_c t$, $\bar{\boldsymbol{p}} = \boldsymbol{p}/mc$, $\bar{\boldsymbol{B}} = \boldsymbol{B}/B_0$ and $\bar{\boldsymbol{E}} = \boldsymbol{E}/cB_0$. Equation (2.3) changes to

$$\frac{\mathrm{d}\bar{\boldsymbol{p}}'}{\mathrm{d}\bar{t}'} = -\bar{E}_0\hat{x} - \frac{\bar{\boldsymbol{p}}'}{\gamma'} \times \left(\hat{x} + \bar{\boldsymbol{B}}'_\perp\right). \tag{3.1}$$

With $E_0 \neq 0$, γ' is no longer constant, so particle motion in $\left(\xi, \mathrm{d}\xi/\mathrm{d}\bar{t}'\right)$ space is no longer conservative. Nevertheless, a new pseudo-energy equation can be derived

https://doi.org/10.1017/S0022377826101998 Published online by Cambridge University Press

exactly (detailed derivation in Appendix A) and is

$$\frac{1}{2}\left(\gamma'\frac{\mathrm{d}\xi}{\mathrm{d}\bar{t}'}\right)^2+\Psi(\xi,\bar{t}')\equiv W_{\mathrm{tot}}=\mathrm{const.},\tag{3.2}$$

where the generalised pseudo-potential $\Psi(\xi,\bar{t}')$ is

$$\Psi(\xi,\bar{t}')\equiv\frac{1}{8}\xi^4+\frac{1}{2}\left[b'^2-\bar{E}_0^2-b'n_{\mathrm{c}}'\bar{p}_{z0}'-\frac{1}{2}\xi_0^2+n_{\mathrm{c}}'\bar{E}_0\int_0^{\bar{t}'}\xi(\bar{\tau}')\mathrm{d}\bar{\tau}'\right]\xi^2$$
$$-\left(b'^2-\bar{E}_0^2\right)\xi-\frac{1}{2}n_{\mathrm{c}}'\bar{E}_0\int_0^{\bar{t}'}\xi^3(\bar{\tau}')\,\mathrm{d}\bar{\tau}',\tag{3.3}$$

and $n_{\mathrm{c}}'=ck'/\omega_{\mathrm{c}}$. Note that $\Psi=\psi$ for $E_0=0$.

Let us first examine particle dynamics far from resonance so that ξ and ξ_0 are much larger than any other variable in (3.3). Dropping terms with b'^2, b' and $\bar{E}_0^2$ in (3.3) and solving for $\mathrm{d}\Psi/\mathrm{d}\bar{t}'=0$ yields

$$\xi_{\mathrm{far}}\simeq\xi_0-n_{\mathrm{c}}'\bar{E}_0\bar{t}'.\tag{3.4}$$

The pseudo-kinetic-energy in (3.2) is then of order $\bar{E}_0^2$ and thus can be dropped. Equation (3.4) is the approximate solution for $\xi(\bar{t}')$ far away from $\xi=0$, and is the result of the particle being unaffected by the wave and only affected by $\bar{E}_0$ in (3.1) so that $\mathrm{d}\bar{p}_x'/\mathrm{d}\bar{t}'=-\bar{E}_0$ or, equivalently, $\mathrm{d}\xi/\mathrm{d}\bar{t}'=-n_{\mathrm{c}}'\bar{E}_0$.

As $\bar{t}'\to\xi_0/n_{\mathrm{c}}'\bar{E}_0$, the particle approaches resonance ($\xi=0$). Because $\xi_0^2/2-n_{\mathrm{c}}'\bar{E}_0\int_0^{\bar{t}'}\xi_{\mathrm{far}}(\bar{\tau}')\,\mathrm{d}\bar{\tau}'\simeq\xi_{\mathrm{far}}^2/2$, the quadratic coefficient in (3.3) becomes $(b'^2-\bar{E}_0^2-b'n_{\mathrm{c}}'\bar{p}_{z0}')/2$ as $\xi\to0$. For a sufficiently large wave amplitude b', this coefficient remains positive, ensuring that Ψ traps the particle near $\xi=0$. If b' is not sufficiently large, the coefficient turns negative, the particle is not trapped by the wave and $\xi\to-\infty$ by (3.4). Since the behaviour of the integral terms becomes nonlinear near $\xi=0$, determining the exact trapping condition turns out to be rather intractable and is left for future work. Here, we focus on the behaviour of the trapped particle.

Finally, we examine the dynamics of said resonance-trapped particle, whose ξ oscillates around $\xi=0$. From the definition of ξ in (2.4), trapping implies that the particle $\bar{p}_x'$ oscillates around a constant value $\bar{p}_{\mathrm{r}}'=-n_{\mathrm{c}}'^{-1}$. Consequently, the bounce-averaged parallel momentum satisfies $\langle\bar{p}_x'\rangle=-n_{\mathrm{c}}'^{-1}$ and $\mathrm{d}\langle\bar{p}_x'\rangle/\mathrm{d}\bar{t}'=0$. Dotting (3.1) with $\bar{\boldsymbol{p}}'$, bounce-averaging and finally using $\mathrm{d}\langle\bar{p}_x'^2\rangle/\mathrm{d}\bar{t}'=\mathrm{d}\langle\bar{p}_x'\rangle^2/\mathrm{d}\bar{t}'$, we obtain solutions for the wave-frame momenta:

$$\langle\bar{p}_\perp'\rangle=\sqrt{\bar{p}_{\perp\mathrm{t}}'^2+\frac{2\bar{E}_0}{n_{\mathrm{c}}'}\left(\bar{t}'-\bar{t}_{\mathrm{t}}'\right)},\quad\langle\bar{p}_x'\rangle=-\frac{1}{n_{\mathrm{c}}'},\tag{3.5}$$

where $\bar{t}_{\mathrm{t}}'$ and $\bar{p}_{\perp\mathrm{t}}'$ are the wave-frame time and perpendicular momentum at which the particle is resonance-trapped. Equation (3.5) shows a surprising result that, once the particle is resonance-trapped, the parallel electric field E_0 energises the particle exclusively in the perpendicular direction and does not contribute to the average parallel momentum in the wave frame.

Now let us transform back to the laboratory frame. Because $\gamma'^2=1+\bar{p}_x'^2+\bar{p}_\perp'^2$, $\mathrm{d}\langle\gamma'^2\rangle/\mathrm{d}\bar{t}'=\mathrm{d}\langle\bar{p}_\perp'^2\rangle/\mathrm{d}\bar{t}'$ for a resonance-trapped particle and so $\langle\gamma'\rangle=$

https://doi.org/10.1017/S0022377826101998 Published online by Cambridge University Press

$\sqrt{\gamma_{\mathrm{t}}'^2 + 2\bar{E}_0(\bar{t}' - \bar{t}_{\mathrm{t}}')/n_{\mathrm{c}}'}$, where γ_{t}' is the wave-frame Lorentz factor at trapping time. Using the Lorentz transformation $\bar{p}_x = (1 - n^{-2})^{-1/2}(\bar{p}_x' + \gamma'/n)$ and bounce-averaging, we obtain solutions for the laboratory-frame momenta:

$$\langle \bar{p}_\perp \rangle = \langle \bar{p}_\perp' \rangle,$$
$$\langle \bar{p}_x \rangle = \frac{1}{\sqrt{1 - n^{-2}}} \left(-\frac{1}{n_{\mathrm{c}}'} + \frac{1}{n} \sqrt{\gamma_{\mathrm{t}}'^2 + \frac{2\bar{E}_0}{n_{\mathrm{c}}'} \left(\bar{t}' - \bar{t}_{\mathrm{t}}' \right)} \right), \tag{3.6}$$

which show another surprising result that once the particle is resonance-trapped, the particle is accelerated in the opposite direction to the prior acceleration by $\bar{E}_0$, i.e. the particle is 'reflected' from the resonant momentum $\bar{p}_{\mathrm{r}}$ in parallel momentum space.

Equations (3.4), (3.5) and (3.6) are our main results, which can be summarised as follows. Under the presence of a uniform magnetic field, a transverse R-wave and a parallel electric field, a negatively charged particle initially far from resonance is accelerated by the electric field towards resonance without being affected much by the wave. Near resonance, the particle is trapped in resonance space if the wave amplitude is large enough. This trapped particle surprisingly experiences net acceleration in the perpendicular direction and also in the parallel direction opposite to its prior acceleration, i.e. it is reflected away from the resonant momentum. Therefore, the R-wave acts as a 'firewall' in parallel momentum space, preventing further acceleration by the parallel electric field beyond the resonant momentum.

4. Single-particle simulation

To verify and visualise the above predictions, we performed single-particle simulations using the relativistic Boris algorithm (Birdsall & Langdon 2004). Equation (3.1) is solved for an electron in the wave frame with an electric field amplitude $\bar{E}_0 = 3.55 \times 10^{-5}$. In this configuration, all electrons are resonantly trapped for $b > 4.75 \times 10^{-4}$, whereas all electrons pass through resonance for $b < 3.9 \times 10^{-4}$. For intermediate amplitudes, trapping depends on the initial phase $\phi_0 \equiv \sin^{-1}(\bar{p}_{z0}/\bar{p}_\perp)$. We consider two representative cases: $b = 5.0 \times 10^{-4}$ (trapped) and $b = 3.5 \times 10^{-4}$ (passing). The wave frequency and the wavenumber are set to $\bar{\omega} \equiv \omega/\omega_{\mathrm{c}} = 0.152$ and $n_{\mathrm{c}} \equiv ck/\omega_{\mathrm{c}} = 0.196$, consistent with the whistler wave dispersion relation for the resonant energy $\gamma_{\mathrm{r}} = 3$ and the normalised electron plasma frequency $\bar{\omega}_{\mathrm{p}} \equiv \sqrt{en_0/\varepsilon_0 m}/\omega_{\mathrm{c}} = 0.290$. These parameters correspond to $n = 1.28$, $b' = 3.16 \times 10^{-4}$ (trapped), $b' = 2.20 \times 10^{-4}$ (passing) and $n_{\mathrm{c}}' = 0.123$. The initial momenta are chosen as $\bar{p}_{x0}' = -6.10$ and $\bar{p}_{z0}' = 0.141$, corresponding to $\xi_0 = 0.25$. For this set-up, the resonant momentum is $\bar{p}_{\mathrm{r}}' = -n_{\mathrm{c}}'^{-1} = -8.13$ in the wave frame and $\bar{p}_{\mathrm{r}} = -2.79$ in the laboratory frame with $\alpha = 0$. A reference simulation with $E_0 = 0$ and different particle parameters is also performed for comparison.

Figure 2 illustrates the time evolution of the generalised pseudo-potential $\Psi(\xi, \bar{t}') - W_{\mathrm{tot}}$. Each circle in the figure represents the electron's position in $\Psi - \xi$ space. For the reference $E_0 = 0$ case (figure 2*a*), $\Psi(\xi, \bar{t}')$ reduces to $\psi(\xi)$; its shape remains constant and is determined solely by the initial conditions, and the electron oscillates in ξ-space in this ψ. Figures 2(*b*) and 2(*c*) show the evolution of Ψ for the case $\bar{E}_0 = 3.55 \times 10^{-5}$ and $b = 5.0 \times 10^{-4}$. As predicted by (3.3)–(3.4), the magnitude of the negative quadratic coefficient decreases with time (figure 2*b*). Near resonance (figure 2*c*), the quadratic coefficient of Ψ becomes positive, resulting in a

https://doi.org/10.1017/S0022377826101998 Published online by Cambridge University Press

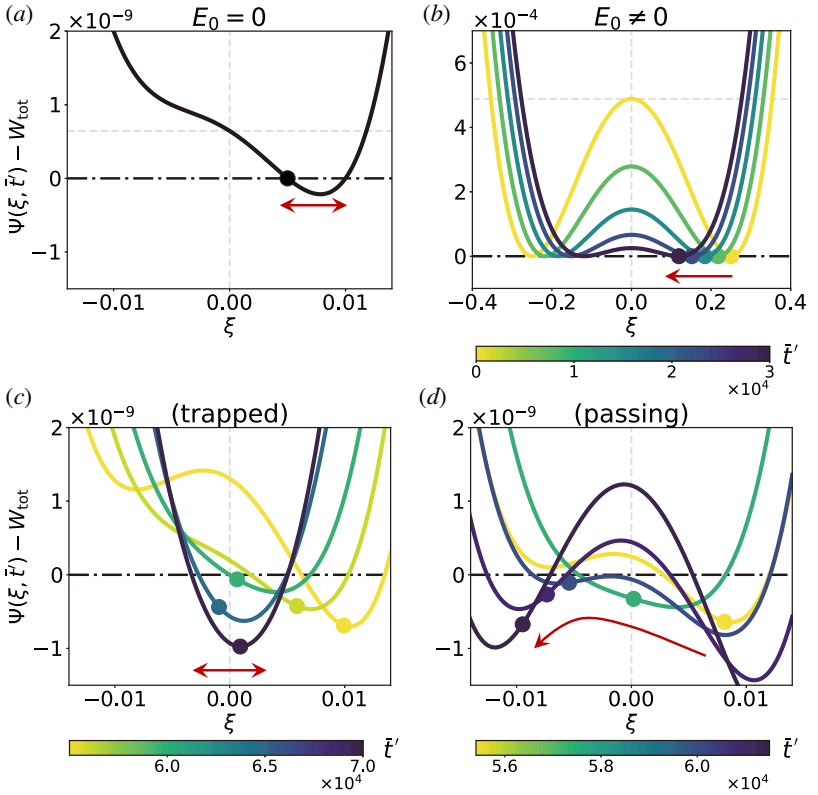


FIGURE 2. Time evolution of $\Psi(\xi, \bar{t}') - W_{\rm tot}$ for (*a*) $E_0 = 0$, (*b*) $\bar{E}_0 = 3.55 \times 10^{-5}$ and $b = 5.0 \times 10^{-4}$, (*c*) same as (*b*) and (*d*) $\bar{E}_0 = 3.55 \times 10^{-5}$ and $b = 3.5 \times 10^{-4}$. The circles are electron positions at each time, and the red arrows qualitatively describe electron motion.

single-well potential that traps the electron around $\xi = 0$. In contrast, for a passing electron with $\bar{E}_0 = 3.55 \times 10^{-5}$ and $b = 3.5 \times 10^{-4}$ (figure 2*d*), the quadratic coefficient returns to a negative value, and the electron transits to the left well of the pseudo-potential.

Figure 3(*a*) shows the time-dependent electron trajectory in ξ-space. Consistent with figure 2(*c*), the trapped electron oscillates around $\xi = 0$. The passing electron, which continues towards $\xi \to -\infty$, is shown for reference. In $\bar{p}'_\perp - \bar{p}'_x$ space (figure 3*b*), $\langle \bar{p}'_x \rangle$ is fixed to $-n'^{-1}_{\rm c}$ as predicted by (3.5), and only $\langle \bar{p}'_\perp \rangle$ increases in time. Figure 3(*c*) shows the electron trajectory in the laboratory-frame $\bar{p}_\perp - \bar{p}_x$ space. As predicted in (3.6), $\bar{p}_x$ reverses direction, opposite to the electric force, while $\bar{p}_\perp$ continues to increase. These electron trajectories in full three-dimensional momentum space correspond to those in figure 1, albeit sparse-sampled for better presentation.

5. Particle-in-cell simulation

Let us now check whether the single-particle mechanism is robust with respect to self-consistent PIC simulations. We verify the firewall effect with the open-source PIC code SMILEI (Derouillat *et al.* 2018), in the context of runaway electrons in tokamak plasmas with a background magnetic field $B_0 = 3.5$ [T], electron density

https://doi.org/10.1017/S0022377826101998 Published online by Cambridge University Press

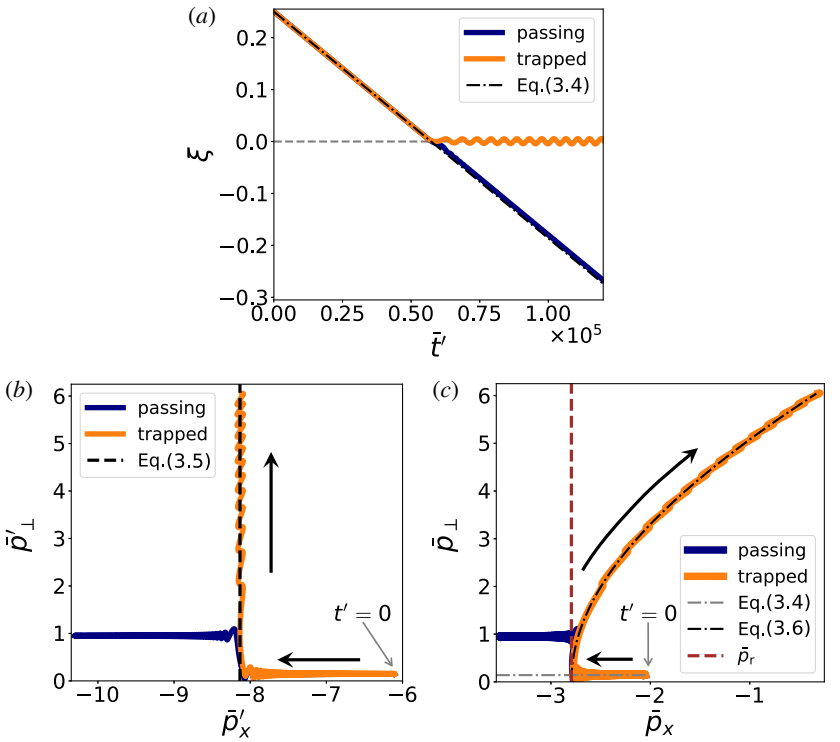


FIGURE 3. (*a*) Time evolution of ξ, (*b*) electron trajectory in $\bar{p}'_\perp - \bar{p}'_x$ space and (*c*) electron motion in $\bar{p}_\perp - \bar{p}_x$ space. The red vertical dashed line in (*c*) indicates the resonant momentum $\bar{p}_\mathrm{r}$ with $\alpha = 0$. The black arrows indicate the direction of electron trajectory. Note that p_x changes opposite to the electrostatic force in the laboratory frame.

$n_0 = 10^{19}$ [m^{-3}] and bulk electron temperature $T_{\mathrm{e}0} = 1$ [keV]. A two-dimensional slab geometry with periodic boundary conditions is assumed, and the field profile modelling an externally injected wave is prescribed as (2.1), with the same wave parameters as for the single-particle simulation. To avoid numerical instabilities arising from uniform electric field acceleration, we benchmark a recent study modelling wave generation by runaway electrons (Kang *et al.* 2024) where the plasma consists of immobile ions and electrons with a bump-on-tail momentum distribution; the latter undergoes an instability and forms a tail distribution, similar to the actual runaway distribution (Paz-Soldan *et al.* 2017; Lvovskiy *et al.* 2018, 2019). The initial bump population density is set to $n_0/16$, with average momenta $\bar{p}_{x0,\mathrm{bump}} = -1.11$ and $\bar{p}_{\perp 0,\mathrm{bump}} = 0.11$. All species are assumed collisionless and uniformly distributed in configuration space. We simulate two cases: (i) with an applied wave ($b = 5 \times 10^{-4}$) and (ii) without a wave ($b = 0$). Further details of the simulation set-up are provided in Appendix B.

Figure 4 shows snapshots of the electron distribution function $f_\mathrm{e}(\bar{p}_x, \bar{p}_y, \bar{t})$ – note that $\bar{p}_y$ is a proxy for $\bar{p}_\perp$. During $\bar{t} = 0 \sim 500$, electrons are accelerated towards the target momentum in both cases as the bump-on-tail instability progresses. For $\bar{t} > 500$, the case without wave has a significant population of electrons that are accelerated beyond $\bar{p}_\mathrm{r}$. However, for the case with wave, most electrons are reflected from $\bar{p}_\mathrm{r}$ and experience enhanced pitch-angle scattering. Comparing

https://doi.org/10.1017/S0022377826101998 Published online by Cambridge University Press

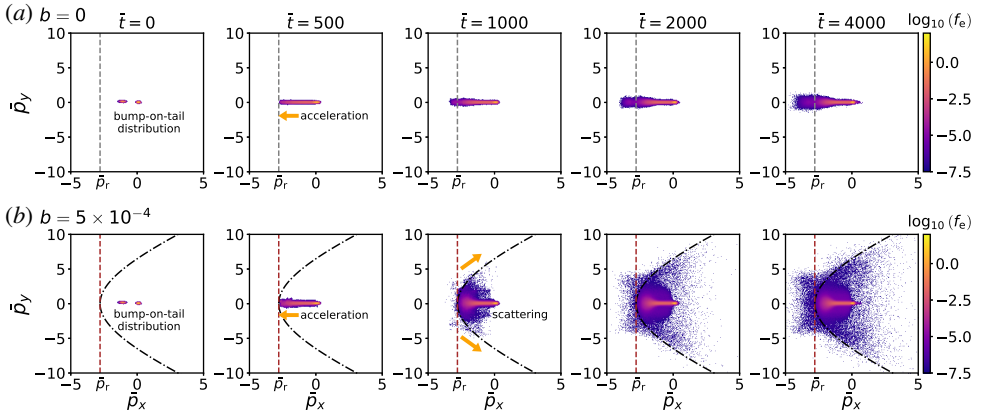


FIGURE 4. Snapshots of electron momentum distribution $f_e(\bar{p}_x, \bar{p}_y, \bar{t})$ from the PIC simulation for the cases (*a*) without external wave and (*b*) with wave. The black dash-dotted lines in (*b*) correspond to (3.6) substituting $\bar{p}'_{\perp t} = \bar{p}_{\perp 0,\mathrm{bump}}$ and $\bar{t}'_t = \xi_0/n'_c\bar{E}_0$, with $\xi_0 = 1 + n'_c\ \bar{p}_{x0,\mathrm{bump}}$ and $\bar{E}_0 = \langle \bar{E}_{x,\mathrm{rms}} \rangle \simeq 8.11 \times 10^{-3}$, and grey or red vertical dashed lines in snapshots refer to $\bar{p}_r$ with $\alpha = 0$.

the two cases, it is clear that the wave suppresses parallel acceleration beyond the resonant momentum via prompt scattering and back-acceleration. In figure 4(*b*), electrons are scattered along the black dash-dotted line, which corresponds to (3.6) substituting $\bar{p}'_{\perp t} = \bar{p}_{\perp 0,\mathrm{bump}}$ and $\bar{t}'_t = \xi_0/n'_c\bar{E}_0$ (from (3.4)), with $\xi_0 = 1 + n'_c\ \bar{p}_{x0,\mathrm{bump}}$ and $\bar{E}_0 = \langle \bar{E}_{x,\mathrm{rms}} \rangle \simeq 8.11 \times 10^{-3}$, where $\bar{E}_{x,\mathrm{rms}} = [\bar{L}_x^{-1}\bar{L}_y^{-1}\int_0^{\bar{L}_y} \mathrm{d}\bar{y} \int_0^{\bar{L}_x} \mathrm{d}\bar{x}(\bar{E}_x^2)]^{1/2}$. This confirms that the scattering mechanism observed in the simulation aligns with the single-particle theoretical prediction.

Quantitatively, the energetic electron population density with $|\bar{p}_x| > |\bar{p}_r|$, $n_{EE} \equiv \int_0^\infty \mathrm{d}\bar{p}_\perp \int_{-\infty}^{\bar{p}_r} \mathrm{d}\bar{p}_x(f_e)$, is reduced by 87 %, and the root-mean-square value of $\bar{p}_y$, $\bar{p}_{y,\mathrm{EE,rms}} \equiv [n_{EE}^{-1}\int_0^\infty \mathrm{d}\bar{p}_\perp \int_{-\infty}^{\bar{p}_r} \mathrm{d}\bar{p}_x(\bar{p}_y^2 f_e)]^{1/2}$, increases by about 516 %, compared with the case without wave. Therefore, an externally injected wave can dramatically limit the momenta of runaways and scatter their pitch angles.

6. Discussion and summary

Quasilinear diffusion is frequently invoked to describe the evolution of runaway distribution in tokamaks (Pokol *et al.* 2008; Guo *et al.* 2018; Liu *et al.* 2018). Although quasilinear theory does not apply for coherent waves, let us nonetheless compare the pitch-angle scattering time scale inferred from the simulation results with that predicted by quasilinear diffusion theory. Using the saturation time of n_{EE} and $\langle \bar{p}_y^2 \rangle_{EE}$, we estimate a characteristic pitch-angle scattering time of $\bar{\tau}_{\alpha,\mathrm{sim}} \sim 10^3$. On the other hand, applying the quasilinear diffusion coefficient of pitch-angle scattering $D_{\alpha\alpha}$ using equation (36) in Summers (2005), evaluated for a Gaussian centred at $\bar{\omega} = 0.152$ with standard deviation $\Delta\bar{\omega} = 0.05$, yields $\bar{D}_{\alpha\alpha} \sim 5 \times 10^{-10}$ and $\bar{\tau}_{\alpha,\mathrm{QL}} \sim 1/D_{\alpha\alpha} \simeq 2 \times 10^9$. Thus, pitch-angle scattering induced by the coherent R-wave proceeds roughly 10^6 times faster than expected from quasilinear diffusion, hinting at the potential for an extremely rapid runaway-suppression method.

We next estimate the power required to compensate for the collisional damping of the wave inside a tokamak (Aleynikov & Breizman 2015; Guo *et al.* 2018;

https://doi.org/10.1017/S0022377826101998 Published online by Cambridge University Press

Yoon *et al.* 2021). For representative tokamak disruption parameters ($B_0 = 3.5$ [T], $n_0 = 10^{19}$ [m^{-3}], $T_{e0} = 100$ [eV], $Z = 1$), the electron–ion collision frequency and R-wave damping rate are $\nu_{ei} \simeq 0.428$ [MHz] and $|\omega_i|/2\pi \simeq 7.13$ [kHz], respectively. Using the power balance equation $P = (|\omega_i|/2\pi)(b^2 B_0^2/2\mu_0)V_p$ and the KSTAR plasma volume $V_p = 17.8$ [m^3], we obtain required power of approximately $P \simeq 155$ [kW]. Because of the rapid interaction, the applied wave only needs to fill a small part of the volume, and so this value is a vast overestimation and thus represents an upper bound. However, the injection efficiency of R-waves or whistler waves to the tokamak core remains an open question, as one may require complicated methods such as mode conversion to achieve this feat.

It should be noted that although a constant electric field was assumed in the theoretical analysis, the parallel field in the PIC simulation is a wave field arising from bump-on-tail instability (snapshots of the electric field are shown in Appendix B). The fact that the same firewall effect was observed in the latter means that the mechanism is robust to small changes in the spatiotemporal nature of the parallel electric field.

For further fusion contexts, if (2.2) is assumed to be in the laboratory frame, it simply describes a current-free twisted magnetic field profile akin to the local field profile in stellarators, with k' encapsulating information about the rotational transform. Therefore, although the present set-up is much simpler, the firewall effect is likely present in stellarators as well. This means that, given appropriate conditions, the presence of a parallel electric field in stellarators may induce perpendicular energisation and perhaps deconfinement, and further investigation is thus warranted. In mirror devices, the present mechanism may be leveraged to increase the pitch angles of particles and push them away from the loss cone.

In space, it is well known that energetic particles in the magnetosphere can resonantly interact with coherent circularly polarised waves and undergo significant pitch-angle scattering (Bellan 2013; Yoon & Bellan 2020). In previous studies, parallel electric fields would naturally have been thought of as a mechanism to decrease the pitch angles of the particles. As we clearly show here, parallel electric fields in fact increase the pitch angles of resonantly trapped particles, and so the present firewall effect warrants a revisiting of the particle scattering theories in space contexts.

In summary, we have identified a counterintuitive firewall effect in which a coherent right-handed circularly polarised wave, combined with a constant parallel electric field, reverses the parallel acceleration direction of an electron and also accelerates it in the perpendicular direction, once it is trapped in Doppler-shifted cyclotron resonance. Single-particle simulations and self-consistent PIC simulations corroborate this mechanism, demonstrating its ability to suppress further runaway-electron acceleration in fusion-relevant conditions. More broadly, the underlying mechanism provides a novel perspective on resonant pitch-angle scattering in magnetised plasmas – from tokamaks and stellarators to astrophysical and space environments.

Acknowledgements

The computational resources for the simulations were provided by the KAIROS supercomputing system at the Korea Institute of Fusion Energy (KFE). This work was supported by the National Research Foundation (NRF) of Korea, grant nos. RS-2022-00154676, RS-2023-00281272, RS-2024-00409564 (G.S.Y. and H.L.K.), RS-2025-00522068 (Y.D.Y.) and RS-2024-00455499 (M.-H.C.). Y.D.Y. was supported by an appointment to the JRG programme at the APCTP through the

https://doi.org/10.1017/S0022377826101998 Published online by Cambridge University Press

Science and Technology Promotion Fund of the Korean Government. Y.D.Y. was also supported by the Korean Local Governments – Gyeongsangbuk-do Province and Pohang City.

Editor Tünde Fülöp thanks the referees for their advice in evaluating this article.

Declaration of interests

The authors report no conflict of interest.

Appendix A. Derivation of the pseudo-energy equation

Here, we derive (3.2)–(3.3) in the main text. Separating the equation of motion in the wave frame (2.3) into the parallel and perpendicular directions, we obtain

$$\frac{\mathrm{d}\bar{p}'_x}{\mathrm{d}\bar{t}'} = -\bar{E}_0 - \hat{x}\cdot\frac{\bar{\boldsymbol{p}}'_\perp}{\gamma'}\times\bar{\boldsymbol{B}}'_\perp, \tag{A1}$$

$$\frac{\mathrm{d}\bar{\boldsymbol{p}}'_\perp}{\mathrm{d}\bar{t}'} = -\frac{\bar{\boldsymbol{p}}'_\perp}{\gamma'}\times\hat{x} - \frac{\bar{p}'_x}{\gamma'}\hat{x}\times\bar{\boldsymbol{B}}'_\perp. \tag{A2}$$

The time derivative of (A1) is

$$\frac{\mathrm{d}^2\bar{p}'_x}{\mathrm{d}\bar{t}'^2} = -\hat{x}\cdot\left\{\left[\bar{\boldsymbol{p}}'_\perp\frac{\mathrm{d}}{\mathrm{d}\bar{t}'}\left(\frac{1}{\gamma'}\right)+\frac{1}{\gamma'}\frac{\mathrm{d}\bar{\boldsymbol{p}}'_\perp}{\mathrm{d}\bar{t}'}\right]\times\bar{\boldsymbol{B}}'_\perp+\frac{\bar{\boldsymbol{p}}'_\perp}{\gamma'}\times\frac{\mathrm{d}\bar{\boldsymbol{B}}'_\perp}{\mathrm{d}\bar{t}'}\right\}. \tag{A3}$$

Using (A2) and the relations

$$\begin{aligned}
\frac{1}{2}\frac{\mathrm{d}\bar{p}'^2}{\mathrm{d}\bar{t}'} &= \bar{\boldsymbol{p}}'\cdot\frac{\mathrm{d}\bar{\boldsymbol{p}}'}{\mathrm{d}\bar{t}'} = -\bar{E}_0\bar{p}'_x,\\
\frac{\mathrm{d}}{\mathrm{d}\bar{t}'}\left(\frac{1}{\gamma'}\right) &= -\frac{1}{2\gamma'^3}\frac{\mathrm{d}\bar{p}'^2}{\mathrm{d}\bar{t}'} = \frac{\bar{E}_0\bar{p}'_x}{\gamma'^3},\\
\hat{x}\cdot\frac{\bar{\boldsymbol{p}}'_\perp}{\gamma'}\times\bar{\boldsymbol{B}}'_\perp &= -\left(\bar{E}_0+\frac{\mathrm{d}\bar{p}'_x}{\mathrm{d}\bar{t}'}\right)
\end{aligned} \tag{A4}$$

and

$$\begin{aligned}
\frac{\mathrm{d}\bar{\boldsymbol{B}}'_\perp}{\mathrm{d}\bar{t}'} &= \frac{\mathrm{d}}{\mathrm{d}\bar{t}'}b'[\hat{y}\sin(k'x')+\hat{z}\cos(k'x')]\\
&= -n'_{\mathrm{c}}\frac{\bar{p}'_x}{\gamma'}\hat{x}\times\bar{\boldsymbol{B}}'_\perp,
\end{aligned} \tag{A5}$$

(A3) becomes

$$\frac{\mathrm{d}^2\bar{p}'_x}{\mathrm{d}\bar{t}'^2} = \frac{1}{\gamma'^2}\left[\bar{E}_0\bar{p}'_x\left(\bar{E}_0+\frac{\mathrm{d}\bar{p}'_x}{\mathrm{d}\bar{t}'}\right)+\left(1+n'_{\mathrm{c}}\bar{p}'_x\right)(\bar{\boldsymbol{p}}'_\perp\cdot\bar{\boldsymbol{B}}'_\perp)-\bar{p}'_x b'^2\right]. \tag{A6}$$

At this point, we utilise the definition of the frequency mismatch parameter in (2.4) and also note that

$$\frac{\mathrm{d}\bar{p}'_x}{\mathrm{d}\bar{t}'} = \frac{1}{n'_{\mathrm{c}}}\frac{\mathrm{d}\xi}{\mathrm{d}\bar{t}'}. \tag{A7}$$

https://doi.org/10.1017/S0022377826101998 Published online by Cambridge University Press

From the time derivative of $\bar{\boldsymbol{p}}'_{\perp} \cdot \bar{\boldsymbol{B}}'_{\perp}$, we obtain

$$\begin{aligned}\frac{\mathrm{d}}{\mathrm{d}\bar{t}'}\left(\bar{\boldsymbol{p}}'_{\perp} \cdot \bar{\boldsymbol{B}}'_{\perp}\right) &= \frac{\mathrm{d}\bar{\boldsymbol{p}}'_{\perp}}{\mathrm{d}\bar{t}'} \cdot \bar{\boldsymbol{B}}'_{\perp} + \bar{\boldsymbol{p}}'_{\perp} \cdot \frac{\mathrm{d}\bar{\boldsymbol{B}}'_{\perp}}{\mathrm{d}\bar{t}'} \\ &= \left(1 + n'_{\mathrm{c}}\bar{p}'_{x}\right)\left(\hat{x} \cdot \frac{\bar{\boldsymbol{p}}'_{\perp}}{\gamma'} \times \bar{\boldsymbol{B}}'_{\perp}\right) \\ &= -\xi\left(\bar{E}_0 + \frac{\mathrm{d}\bar{p}'_{x}}{\mathrm{d}\bar{t}'}\right) \\ &= -\bar{E}_0\xi - \frac{1}{2n'_{\mathrm{c}}}\frac{\mathrm{d}\xi^2}{\mathrm{d}\bar{t}'}. \end{aligned} \tag{A8}$$

Integrating over time and using $\bar{\boldsymbol{p}}'_{\perp} \cdot \bar{\boldsymbol{B}}'_{\perp}|_{\bar{t}'=0} = b'\bar{p}'_{z0}$,

$$\bar{\boldsymbol{p}}'_{\perp} \cdot \bar{\boldsymbol{B}}'_{\perp} = b'\bar{p}'_{z0} - \bar{E}_0\int_0^{\bar{t}'} \xi(\bar{\tau}')\mathrm{d}\bar{\tau}' - \frac{1}{2n'_{\mathrm{c}}}\left(\xi^2 - \xi_0^2\right). \tag{A9}$$

Using the above and replacing all $\bar{p}'_x$ by $n'^{-1}_{\mathrm{c}}(\xi - 1)$, (A6) becomes

$$\begin{aligned}\gamma'^2\frac{\mathrm{d}^2\xi}{\mathrm{d}\bar{t}'^2} &= (\xi - 1)\bar{E}_0\left(\bar{E}_0 + \frac{1}{n'_{\mathrm{c}}}\frac{\mathrm{d}\xi}{\mathrm{d}\bar{t}'}\right) - (\xi - 1)\,b'^2 \\ &\quad + \xi\left[b'n'_{\mathrm{c}}\bar{p}'_{z0} - n'_{\mathrm{c}}\bar{E}_0\int_0^{\bar{t}'} \xi(\bar{\tau}')\,\mathrm{d}\bar{\tau}' - \frac{1}{2}\left(\xi^2 - \xi_0^2\right)\right]. \end{aligned} \tag{A10}$$

Using

$$\begin{aligned}\frac{1}{2}\frac{\mathrm{d}\gamma'^2}{\mathrm{d}\bar{t}'} = \frac{1}{2}\frac{\mathrm{d}\bar{p}'^2_{x}}{\mathrm{d}\bar{t}'} &= -\bar{E}_0\bar{p}'_{x} \\ &= -\frac{\bar{E}_0}{n'_{\mathrm{c}}}(\xi - 1) \end{aligned} \tag{A11}$$

and

$$\xi\int_0^{\bar{t}'} \xi(\bar{\tau}')\mathrm{d}\bar{\tau}' = \frac{1}{2}\frac{\partial}{\partial\xi}\left(\xi^2\int_0^{\bar{t}'} \xi(\bar{\tau}')\mathrm{d}\bar{\tau}' - \int_0^{\bar{t}'} \xi^3(\bar{\tau}')\mathrm{d}\bar{\tau}'\right), \tag{A12}$$

we obtain

$$\gamma'^2\frac{\mathrm{d}^2\xi}{\mathrm{d}\bar{t}'^2} = -\frac{1}{2}\frac{\mathrm{d}\gamma'^2}{\mathrm{d}\bar{t}'}\frac{\mathrm{d}\xi}{\mathrm{d}\bar{t}'} - \frac{\partial}{\partial\xi}\Psi(\xi, \bar{t}'), \tag{A13}$$

where the generalised pseudo-potential $\Psi(\xi, \bar{t}')$ is described in (3.3). Multiplying $\mathrm{d}\xi/\mathrm{d}\bar{t}'$ to (A13), and integrating over $\bar{t}'$, we finally obtain the pseudo-energy equation (3.2).

Appendix B. Details of PIC simulation

In this appendix, we present the PIC simulation set-up and the time evolution of the electric fields in more detail. The simulation code and geometry are described

https://doi.org/10.1017/S0022377826101998 Published online by Cambridge University Press

Wave frequency	$\bar{\omega} = 0.152$
Wavenumber	$n_c = 0.196$
Number of cells	$N_{\mathrm{cell},x} = 2^{14}$
	$N_{\mathrm{cell},y} = 2^{9}$
Domain size	$\bar{L}_x = 5\bar{\lambda}$
	$\bar{L}_y = 1.25\bar{\lambda}$
Time step	$\Delta\bar{t} = 9.20 \times 10^{-3}$
Simulation time	$\bar{t}_{\mathrm{sim}} = 5000$
Electron plasma frequency	$\bar{\omega}_p = 0.290$
Initial average momentum (background electron)	$\bar{p}_{x0,\mathrm{BE}} = 0.0495,$ $\bar{p}_{\perp 0,\mathrm{BE}} = 0$
Initial average momentum (bump)	$\bar{p}_{x0,\mathrm{bump}} = -1.11,$ $\bar{p}_{\perp 0,\mathrm{bump}} = 0.11$
Initial bump population	$n_{0,\mathrm{bump}} = n_0/16$
Temperature	$T_{0,\mathrm{BE}} = T_{0,\mathrm{bump}} = 1$ [keV]
Super-particles per cell	$N_{\mathrm{ppc}} = \begin{cases} 64, & \text{for background electron} \\ 32, & \text{for ion, bump} \end{cases}$

TABLE 1. The PIC simulation parameters. Here, $\bar{\lambda} \equiv 2\pi/n_c$.

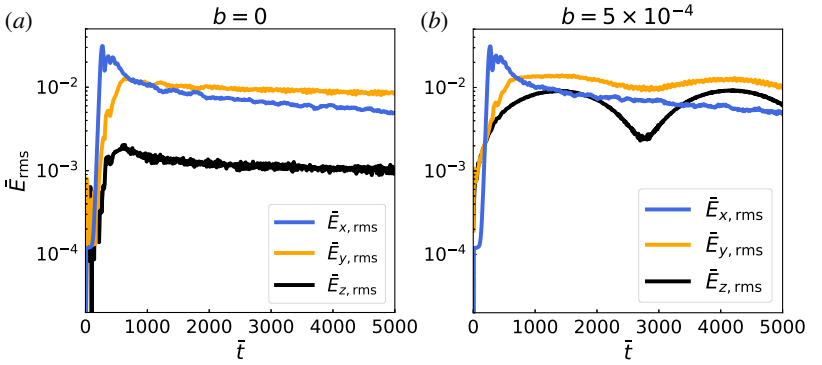


FIGURE 5. Log-scale plots of $\bar{E}_{j,\mathrm{rms}}$ $(j = x, y, z)$ for (a) $b = 0$ and (b) $b = 5 \times 10^{-4}$.

in the main text. In addition, we employ the Lehe field solver (Lehe *et al.* 2013) to mitigate numerical Cherenkov instability. The detailed simulation parameters are summarised in table 1.

Figure 5 shows the evolution of the root-mean-square electric fields $\bar{E}_{j,\mathrm{rms}}$ $(j = x, y, z)$ for $b = 0$ and $b = 5 \times 10^{-4}$. For $\bar{t} < 250$, an electrostatic wave is driven by the relaxation of the bump-on-tail distribution in the x direction (Kang *et al.* 2024). By Maxwell's equations in the two-dimensional geometry ($\Delta z = 0$), $\bar{B}_z$ and $\bar{E}_y$ grow predominantly in time for the $b = 0$ case. In contrast, as shown in figure 5(b), resonant interactions between the R-wave and electrons enhance both $\bar{E}_y$ and $\bar{E}_z$. For $\bar{t} > 1000$, the electric fields saturate at the level $\bar{E}_{\mathrm{rms}} \sim 10^{-3}$. The time-averaged values of $\bar{E}_{x,\mathrm{rms}}$ are $\langle \bar{E}_{x,\mathrm{rms}} \rangle \simeq 8.04 \times 10^{-3}$ for $b = 0$ and $\langle \bar{E}_{x,\mathrm{rms}} \rangle \simeq 8.11 \times 10^{-3}$ for $b = 5 \times 10^{-4}$.

https://doi.org/10.1017/S0022377826101998 Published online by Cambridge University Press

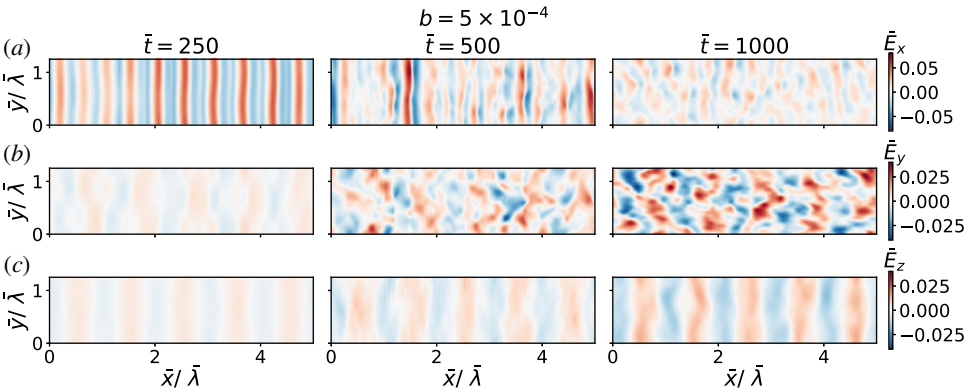


FIGURE 6. Snapshots of (*a*) $\bar{E}_x$, (*b*) $\bar{E}_y$ and (*c*) $\bar{E}_z$ for the $b = 5 \times 10^{-4}$ case. Colourmap indicates the amplitude of electric fields.

We next present snapshots of the electric-field profiles for the case $b = 5 \times 10^{-4}$. Figure 6 shows snapshots of $\bar{E}_x$, $\bar{E}_y$ and $\bar{E}_z$, where $\bar{x} = x\ \omega_c/c$ and $\bar{y} = y\ \omega_c/c$. At $\bar{t} = 250$, $\bar{E}_x$ arises from the relaxation of the bump-on-tail distribution. While some bump electrons are accelerated towards the resonant momentum, others are decelerated and merge with the background population. For $500 \lesssim \bar{t} \lesssim 1000$, the amplitude of $\bar{E}_x$ decreases while its spatial profile remains similar to that at $\bar{t} = 250$, continuing to accelerate energetic electrons. During this phase, $\bar{E}_y$ and $\bar{E}_z$ increase due to the instability itself.

The most important takeaway is the robustness of the resonant interaction with respect to the spatiotemporal variations of the electric field. The $\bar{E}_x$ structure from the bump-on-tail instability is drastically different from a uniform parallel field assumed in the theoretical analysis. There are also additional perpendicular fields that are generated due to the instability on top of the prescribed R-wave. However, electrons are still prevented from accelerating beyond $\bar{p}_r$ as shown in figure 4(*b*), indicating that the firewall effect is still robustly in effect. Therefore, our relatively simple theoretical analysis is still applicable to such self-consistent, more complex situations.

REFERENCES

ALEYNIKOV, P. & BREIZMAN, B. 2015 Stability analysis of runaway-driven waves in a tokamak. *Nucl. Fusion* **55**, 043014.

BELLAN, P.M. 2013 Pitch angle scattering of an energetic magnetized particle by a circularly polarized electromagnetic wave. *Phys. Plasmas* **20**, 042117.

BIRDSALL, C.K. & LANGDON, A.B. 2004 *Plasma Physics via Computer Simulation*. CRC Press.

BREIZMAN, B.N., ALEYNIKOV, P., HOLLMANN, E.M. & LEHNEN, M. 2019 Physics of runaway electrons in tokamaks. *Nucl. Fusion* **59**, 083001.

BURDAKOV, A.V., IVANOV, A.A. & KRUGLYAKOV, E.P. 2010 Modern magnetic mirrors and their fusion prospects. *Plasma Phys. Control. Fusion* **52**, 124026.

CHOUDHURY, H. *et al.* 2026 First demonstration of resonant pitch-angle scattering of relativistic electrons by externally-launched helicon waves. *Phys. Rev. Lett.* **136**, 025101.

COMPERNOLLE, B.V., BORTNIK, J., PRIBYL, P., GEKELMAN, W., NAKAMOTO, M., TAO, X. & THORNE, R.M. 2014 Direct detection of resonant electron pitch angle scattering by whistler waves in a laboratory plasma. *Phys. Rev. Lett.* **112**, 145006.

https://doi.org/10.1017/S0022377826101998 Published online by Cambridge University Press

CONNOR, J.W. & HASTIE, R.J. 1975 Relativistic limitations on runaway electrons. *Nucl. Fusion* **15**, 415.

DECKER, J. *et al.* 2024 Expulsion of runaway electrons using ECRH in the TCV tokamak. *Nucl. Fusion* **64**, 106027.

DEROUILLAT, J. *et al.* 2018 Smilei: a collaborative, open-source, multi-purpose particle-in-cell code for plasma simulation. *Comput. Phys. Commun.* **222**, 351–373.

ERGUN, R.E., ANDERSSON, L., MAIN, D.S., SU, Y.-J., CARLSON, C.W., MCFADDEN, J.P. & MOZER, F.S. 2002 Parallel electric fields in the upward current region of the aurora: indirect and direct observations. *Phys. Plasmas* **9**, 3685–3694.

FÄLTHAMMAR, C.-G. 1989 Electric fields in the magnetosphere—a review. *Planet. Space Sci.* **37**, 899–914.

GELLER, R., HOPFGARTEN, N., JACQUOT, B. & JACQUOT, C. 1974 Electric fields parallel to the magnetic field in a laboratory plasma in a magnetic mirror field. *J. Plasma Phys.* **12**, 467–486.

GUO, Z., MCDEVITT, C.J. & TANG, X.Z. 2018 Control of runaway electron energy using externally injected whistler waves. *Phys. Plasmas* **25**, 032504.

GURNETT, D.A. 1972 Electric field and plasma observations in the magnetosphere. In *Critical Problems of Magnetosphere Physics* (ed. E.R. Dyer), pp. 123–136. National Academy of Sciences.

HEIDBRINK, W.W. & WHITE, R.B. 2020 Mechanisms of energetic-particle transport in magnetically confined plasmas. *Phys. Plasmas* **27**, 030901.

HELANDER, P., ERIKSSON, L.-G. & ANDERSSON, F. 2002 Runaway acceleration during magnetic reconnection in tokamaks. *Plasma Phys. Control. Fusion* **44**, B247–B262.

HORNE, R.B., THORNE, R.M., MEREDITH, N.P. & ANDERSON, R.R. 2003 Diffuse auroral electron scattering by electron cyclotron harmonic and whistler mode waves during an isolated substorm. *J. Geophys. Res.: Space Phys.* **108**, 1290.

INAN, U.S., BELL, T.F., BORTNIK, J. & ALBERT, J.M. 2003 Controlled precipitation of radiation belt electrons. *J. Geophys. Res.: Space Phys.* **108**, 1186.

KANG, H.L., YOON, Y.D., CHO, M.-H. & YUN, G.S. 2024 Fast nonlinear scattering of runaway electron beams through resonant interactions with plasma waves. *Nucl. Fusion* **64**, 106025.

KASAHARA, S. *et al.* 2018 Pulsating aurora from electron scattering by chorus waves. *Nature* **554**, 337–340.

KIROV, K.K. *et al.* 2024 Analysis of fusion alphas interaction with RF waves in D-T plasma at JET. *Nucl. Fusion* **64**, 086011.

KURAMITSU, Y. & KRASNOSELSKIKH, V. 2005*a* Acceleration of charged particles by gyroresonant surfing at quasi-parallel shocks. *Astron. Astrophys.* **438**, 391–402.

KURAMITSU, Y. & KRASNOSELSKIKH, V. 2005*b* Gyroresonant surfing acceleration. *Phys. Rev. Lett.* **94**, 031102.

KURAMITSU, Y. & KRASNOSELSKIKH, V. 2005*c* Particle acceleration by elliptically and linearly polarized waves in the vicinity of quasi-parallel shocks. *J. Geophys. Res.: Space Phys.* **110**, A10108.

LACOMBE, C., ALEXANDROVA, O., MATTEINI, L., SANTOLÍK, O., CORNILLEAU-WEHRLIN, N., MANGENEY, A., CONCHY, Y.D. & MAKSIMOVIC, M. 2014 Whistler mode waves and the electron heat flux in the solar wind: cluster observations. *Astrophys. J.* **796**, 5.

LEE, Y., ALEYNIKOV, P., VRIES, P.C.D., KIM, H.T., LEE, J., HOPPE, M., PARK, J.K., CHOI, G.J., GWAK, J. & NA, Y.S. 2024 Binary nature of collisions facilitates runaway electron generation in weakly ionized plasmas. *Phys. Rev. Lett.* **133**, 175102.

LEHE, R., LIFSCHITZ, A., THAURY, C., MALKA, V. & DAVOINE, X. 2013 Numerical growth of emittance in simulations of laser-wakefield acceleration. *Phys. Rev. ST - Accel. Beams* **16**, 021301.

LIU, C., HIRVIJOKI, E., FU, G.Y., BRENNAN, D.P., BHATTACHARJEE, A. & PAZ-SOLDAN, C. 2018 Role of kinetic instability in runaway-electron avalanches and elevated critical electric fields. *Phys. Rev. Lett.* **120**, 265001.

LVOVSKIY, A., HEIDBRINK, W.W., PAZ-SOLDAN, C., SPONG, D.A., MOLIN, A.D., EIDIETIS, N.W., NOCENTE, M., SHIRAKI, D. & THOME, K.E. 2019 Observation of rapid frequency chirping instabilities driven by runaway electrons in a tokamak. *Nucl. Fusion* **59**, 124004.

LVOVSKIY, A. *et al.* 2018 The role of kinetic instabilities in formation of the runaway electron current after argon injection in DIII-D. *Plasma Phys. Control. Fusion* **60**, 124003.

LYONS, L.R. 1974 Pitch angle and energy diffusion coefficients from resonant interactions with ion–cyclotron and whistler waves. *J. Plasma Phys.* **12**, 417–432.

https://doi.org/10.1017/S0022377826101998 Published online by Cambridge University Press

MARSHALL, R.S. & BELLAN, P.M. 2019 Acceleration of charged particles to extremely large energies by a sub-Dreicer electric field. *Phys. Plasmas* **26**, 042102.

MIYOSHI, Y., KATOH, Y., NISHIYAMA, T., SAKANOI, T., ASAMURA, K. & HIRAHARA, M. 2010 Time of flight analysis of pulsating aurora electrons, considering wave-particle interactions with propagating whistler mode waves. *J. Geophys. Res.: Space Phys.* **115**, A10312.

OMURA, Y., FURUYA, N. & SUMMERS, D. 2007 Relativistic turning acceleration of resonant electrons by coherent whistler mode waves in a dipole magnetic field. *J. Geophys. Res.: Space Phys.* **112**, A06236.

PARK, J.Y., YOON, Y.D. & HWANG, Y.-S. 2025 Kinetic turbulence drives MHD equilibrium change via 3D reconnection. *Nature* **644**, 59–63.

PAUL, E.J., BHATTACHARJEE, A., LANDREMAN, M., ALEX, D., VELASCO, J.L. & NIES, R. 2022 Energetic particle loss mechanisms in reactor-scale equilibria close to quasisymmetry. *Nucl. Fusion* **62**, 126054.

PAUL, E.J., MYNICK, H.E. & BHATTACHARJEE, A. 2023 Fast-ion transport in quasisymmetric equilibria in the presence of a resonant Alfvénic perturbation. *J. Plasma Phys.* **89**, 905890515.

PAZ-SOLDAN, C. *et al.* 2017 Spatiotemporal evolution of runaway electron momentum distributions in tokamaks. *Phys. Rev. Lett.* **118**, 255002.

POKOL, G., FÜLÖP, T. & LISAK, M. 2008 Quasi-linear analysis of whistler waves driven by relativistic runaway beams in tokamaks. *Plasma Phys. Control. Fusion* **50**, 045003.

REAMES, D.V., MEYER, J.P. & VON ROSENVINGE, T.T. 1994 Energetic-particle abundances in impulsive solar flare events. *Intl Astron. Union Colloq.* **142**, 649–667.

RICHARD, L., KHOTYAINTSEV, Y.V., NORGREN, C., STEINVALL, K., GRAHAM, D.B., EGEDAL, J., VAIVADS, A. & NAKAMURA, R. 2025 Electron heating by parallel electric fields in magnetotail reconnection. *Phys. Rev. Lett.* **134**, 215201.

SALEWSKI, M. *et al.* 2025 Energetic particle physics: Chapter 7 of the special issue: on the path to tokamak burning plasma operation. *Nucl. Fusion* **65**, 043002.

SAUVAUD, J.A., MAGGIOLO, R., JACQUEY, C., PARROT, M., BERTHELIER, J.J., GAMBLE, R.J. & RODGER, C.J. 2008 Radiation belt electron precipitation due to vlf transmitters: satellite observations. *Geophys. Res. Lett.* **35**, L09101.

SCHINDLER, K., HESSE, M. & BIRN, J. 1988 General magnetic reconnection, parallel electric fields, and helicity. *J. Geophys. Res.: Space Phys.* **93**, 5547–5557.

SIENA, A.D., BAÑÓN NAVARRO, A. & JENKO, F. 2020 Turbulence suppression by energetic particle effects in modern optimized stellarators. *Phys. Rev. Lett.* **125**, 105002.

STANSBY, D., HORBURY, T.S., CHEN, C.H.K. & MATTEINI, L. 2016 Experimental determination of whistler wave dispersion relation in the solar wind. *Astrophys. J. Lett.* **829**, L16.

SUMMERS, D. 2005 Quasi-linear diffusion coefficients for field-aligned electromagnetic waves with applications to the magnetosphere. *J. Geophys. Res.: Space Phys.* **110**, A08213.

VOCKS, C., SALEM, C., LIN, R.P. & MANN, G. 2005 Electron Halo and Strahl formation in the solar wind by resonant interaction with whistler waves. *Astrophys. J.* **627**, 540.

YEH, H.-C. & HILL, T.W. 1981 Mechanism of parallel electric fields inferred from observations. *J. Geophys. Res.: Space Phys.* **86**, 6706–6712.

YOO, J., NG, J., JI, H., BOSE, S., GOODMAN, A., ALT, A., CHEN, L.-J., SHI, P. & YAMADA, M. 2024 Anomalous resistivity and electron heating by lower hybrid drift waves during magnetic reconnection with a guide field. *Phys. Rev. Lett.* **132**, 145101.

YOON, Y.D. & BELLAN, P.M. 2020 Nondiffusive pitch-angle scattering of a distribution of energetic particles by coherent whistler waves. *J. Geophys. Res.: Space Phys.* **125**, e2020JA027796.

YOON, Y.D., JI, J.Y. & YUN, G.S. 2021 Deterministic scattering of relativistic electron beams by off-resonant circularly polarized electromagnetic waves. *Phys. Plasmas* **28**, 060702.

ZHOU, R.J., HU, L.Q., LU, H.W., LI, E.Z., LIN, S.Y., XU, P. & ZHANG, L. 2011 Generation and suppression of runaway electrons in EAST lower hybrid current drive experiments. *Phys. Scripta* **84**, 015501.

https://doi.org/10.1017/S0022377826101998 Published online by Cambridge University Press